



Structure and age of ancient walls from the city of Nan, northern Thailand

Prapawadee Srisunthon¹ · Daniela Mueller¹ · Jakob Wilk¹ · Frank Preusser¹

Received: 6 July 2023 / Accepted: 26 March 2024
© The Author(s) 2024

Abstract

The structure and age of remains of two ancient walls located in the city of Nan, a former part of the Lanna Kingdom in modern northern Thailand, were investigated. The remains differ in appearance with a well-preserved brick wall present at Mahawong Road (MHW), while an earthwork with a brick reinforcement core is found at Phaya Wat Temple (PWT). We employed an electrical resistivity tomography (ERT) survey and optically stimulated luminescence dating (OSL) to determine the buried structure of the earthwork at the PWT site and the production age of bricks from both locations. The ERT results reveal lateral heterogeneous resistivity domains cross-cutting the wall, which presumably relates to the construction of a dam. According to OSL dating, the PWT wall was likely built during the time of the war with Burma that ultimately resulted in a foreign occupation of Nan in the sixteenth century. This structure played a role in both flood mitigation and military defence of the city. The structure at MHW represents a city wall that was built at the end of the nineteenth century after Nan was relocated to its present position and rather reflects representative and social needs.

Keywords Ancient city wall · Mainland southeast Asia · Nan · Thailand · Lanna · OSL · ERT

Introduction

Ancient city walls of mainland SE Asia provide insights into the rich history of cultural development of human settlements within the region. The concept of living in walled settlements is believed to have arose because of the trade exchange with India and especially China, with whom relationships are documented as early as ca. 2000 BC (Shang Dynasty) (Stuart-Fox 2021). The people of SEA adopted the concept of cities being surrounded by walls in response to the geographical location, in particular the fact that settlements are mainly located on floodplains. Therefore, settlements regularly used natural drainage channels as entrenchments or moats in the overall construction concept. These were regularly accompanied by earthen walls topped by a log stockade and/or stone, laterite, and brick walls (Stark 2006). This urban settlement concept arrived in SEA during the Iron Age (ca. 500 BC) and was probably used until around AD 800, in northeastern Thailand, before city wall

structures were implemented (McGrath and Boyd 2001). According to Miksic and Goh (2017), the “Pyu Ancient City” in the Ayeyarwadi Plain (Irrawaddy) of central Burma is the by far oldest known settlement combining a brick wall and a moat in SEA, dating likely to the first millennium AD. Furthermore, the city walls of SEA were not only used for flood protection, contouring a territory and fortification, but also served as a symbol of civic identity to express power and prestige (Smith 2003; Stark 2006). The kingdoms of SEA originally developed from tribal societies, minorities and craftsman communities, and only later formed states (e.g. White and Pigott 1996). City walls became a status symbol to express the hierarchical mobility in the state formation process such as developing from a village to a city.

Within northern Thailand, the remains of ancient city walls reflect the influence of cultural developments on the human settlement during the Lanna period (13th – seventeenth century AD). City walls and moats are essential features of the Lanna urban fabric. Most of the structures are near vertical or vertical walls enclosed by moats, encircling entire city areas (Wood et al. 2015). Around the fifteenth–sixteenth century AD, the city walls of several towns of the Lanna culture had their earthworks reinforced with brick structures, which might be relate to the increased severity

✉ Prapawadee Srisunthon
ps493@geologie.uni-freiburg.de

¹ Institute of Earth and Environmental Sciences, University of Freiburg, Albertstr. 23B, 79104 Freiburg, Germany

of raids that came along with the introduction of gunpowder from the trade with China during the Ming Dynasty (AD 1368–1644) and the frequency of wars, for example, with Burma and Ho (Laichen 2003; Lertrit 2000). However, it is assumed that city walls and moats in many regions of Thailand, similar to the rest of SEA, had functions beyond simple fortification purposes, especially flood alleviation (e.g. Lertlum 2019; Ng et al. 2015; Parry 1992; Scott and O'Reilly 2015; Wood et al. 2015). In addition, they likely also reflect cultural beliefs in the way they have been designed (e.g. Phetsuriya and Health 2021; Srinurak and Mishima 2017; for further details see “[Historical context](#)”).

In the city of Nan, which flourished during the thirteenth century AD and later became part of the Lanna Kingdom, the remains of two wall structures are found today, which are not fully understood with regard to their function and age as the city has been relocated several times. Fragmentary segments of ancient walls are located in two different parts of the city (Fig. 1), one in the north along Mahawong Road (MHW), and one in the south near the Phaya Wat Temple (PWT), a Buddhist sanctuary with its origin dating back to the sixteenth century AD (Fine Arts Department 2012). While the MHW wall is entirely built of bricks, the PWT wall is an earthwork structure with previous excavations revealing it comprises a buried brick structure (Fine Arts Department 2012). Both PWT and MHW are enclosed by moats which appear to have been natural creeks that were artificially deepened. However, it is yet unknown if the two wall fragments are related to each other, when they were built, and what their function was. Therefore, understanding the internal structure and deciphering the age of the wall fragments will add crucially to the interpretation of the local historical context.

To further our understanding of the region, the subsurface structure of the PWT earthwork site was investigated using electrical resistivity tomography (ERT). Optically stimulated luminescence (OSL) dating was applied to date the production age of bricks from both sites. The overall aim of this study is to contribute to the understanding of the role and function of city walls in the context of the historic cultural development in mainland SEA, hence, firstly the historical context of the region is introduced in detail.

Regional setting

Historical context

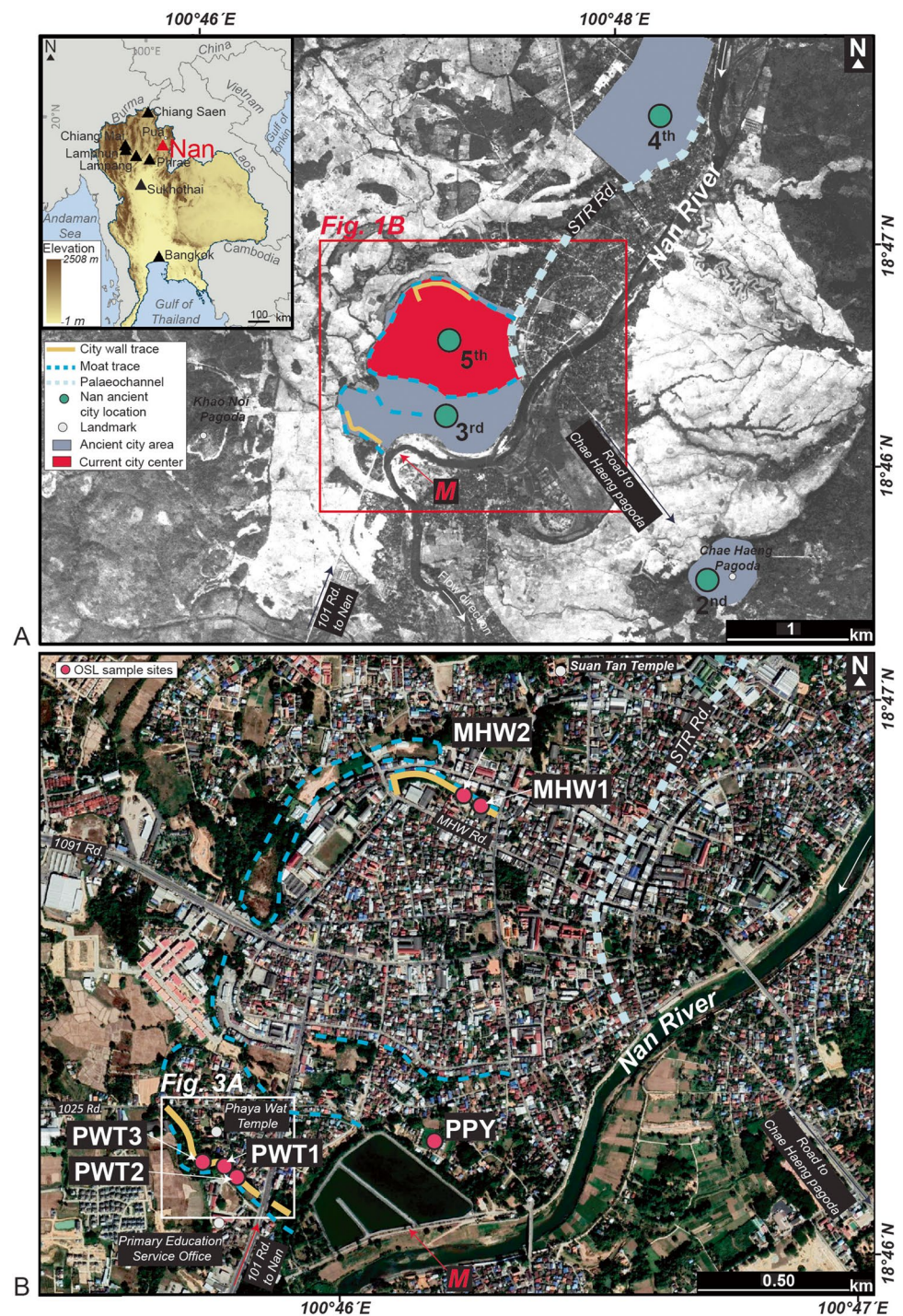
Since the prehistoric period, the settlement morphology of an urban area surrounded by earthworks and moats has been used in SE Asia, in particular in the area of present-day Thailand (e.g. Boyd et al. 1999; Higham 2011; Stark 2006; Welch and McNeill 1988). Several ancient villages

were surrounded by earthworks enclosed by moats, the latter were often natural drainage channels modified by humans to delineate their territorial claims (Boyd et al. 1999; Duke et al. 2016; Murphy 2013; Ongsakul 2005; O'Reilly and Scott 2015). This includes locations in the Mun and Chi river basins in northeastern Thailand (dating to 500 BC to AD 800), in central Thailand (Dvaravadi period, 6th – eleventh century AD), Funan in Vietnam (2nd – twelfth century AD), as well as in northern Thailand (Hariphunchai, 7th – thirteenth century AD, and Lanna period, thirteenth–seventeenth century AD). Numerous hypotheses have been proposed to explain the function of earthworks with moats, for example, defence, water storage, flooding mitigation, water conveyance, agriculture and/or aquaculture, as well as symbolic purposes (Mudar 1999; O'Reilly 2008; Scott and O'Reilly 2015; Srinurak and Mishima 2017; Vallibhotama 1986; Williams-Hunt 1950; Wood et al. 2015). Each of these hypotheses can be challenged on various grounds e.g. anthropology and sociology, and it appears likely that the combination of earthworks and moats served multiple purposes.

During the Lanna period (thirteenth–seventeenth century AD), the location, daily activities, and beliefs were the most important factors for urban settlement concepts in northern Thailand. Some cities were founded along floodplains of rivers whereas others were built on hills or directly on slopes (Ng et al. 2015; Supajanya and Vallibhotama 1972). Srinurak and Mishima (2017) report that Lanna cities were frequently designed in response to essential functions such as defence, festivals, religious purposes, and daily activities such as occupation and transportation. During the Lanna period, numerous communities, including Lamphun, Lamphang, Phrae, Chiang Saen, and Chiang Mai (Fig. 1A), attempted to construct their cities according to their religious beliefs, i.e., using the shape of a “Sankh” (a conch shell) or the “Traiphum Cosmology” (three worlds – heaven, earth, and underworld). People arranged their cities by using walls and moats to contour the shape (Srinurak and Mishima 2017). For example, the ancient city of Chiang Saen, on the southern bank of the Mekong River, built wall constructions leading to the river which itself functioned as a fortification moat (Wyatt and Wichienkeo 1995). Moreover, the Kingdom of Sukhothai (Fig. 1A), an independent kingdom during the Lanna period, also applied a similar urban concept and used moats for water management as the irrigation structure of the higher elevated city area (Vallibhotama 1986).

Historically, Nan is considered an important city within northern Thailand since it started to flourish in the late twelfth century AD and governed the highland tribes (Cheewinsiriwat 2013). The ancient city of Nan was first established in the valley near the source of the Nan River (present day Pua district; Fig. 1). In AD 1450, Nan came under the suzerainty of Lanna, during the reign of King Tilokaraj

Fig. 1 **A** Aerial photo of the modern Nan city area taken in February 1954 with indication of past locations of the city (aerial photo obtained from the Royal Thai Survey Department with 25 m resolution). A meander of the Nan River reaching the location of the ancient wall at the Phaya Wat Temple (PWT) site (location *M* (red) in the figure) is shown. The overview map (inset) shows the regional topography (1-arc second DEM of ASTER (2019); 30 m resolution) and locations of ancient cities during the Lanna period as mentioned in the text. **B** Satellite photo from 6th January 2021 (Google Earth 2021; 30 m resolution) showing locations of ancient walls, moats, and OSL sample locations

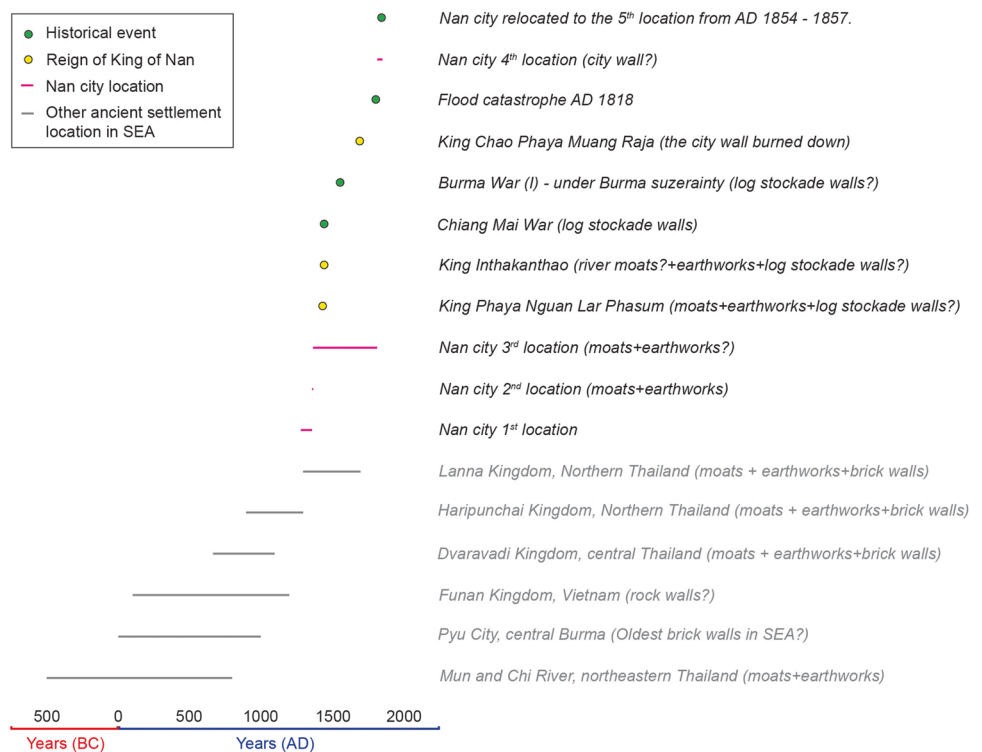


of Chiang Mai (the capital of the Lanna Kingdom; Fig. 1). Inferring from the distribution of archaeological sites and ancient villages, the linear settlement pattern along rivers, which served as transportation lines and ensured a constant water supply, the Nan region is similar to other parts of northern Thailand (Boomgaard 2007; Ng et al. 2015).

Due to the natural hazard of flooding and fluvial landscape change, the ancient city of Nan was relocated four

times between the late twelfth and nineteenth century (Ongsakul 1996; Pharitdet 1918, Fig. 1A and Fig. 2). After the first relocation that occurred from AD 1359–1368, the city was called “Chae Haeng” (Haeng = dry in Thai). This ancient city occupied a hill to the east of the Nan River which is in proximity to the current city location. The movement to the second location was due to the rising population and the ties to Buddhism during the reign of

Fig. 2 Chronology of occurrence of walls in mainland SE Asia and in the Nan area, phase of Nan city settlements at different locations and important historic events



King Phra Ya Kan Muang (AD 1356–1363). A pagoda was built to preserve Buddha relics which were gifted by the Sukhothai Kingdom to express their royal kinship (Nokgam 2018; Pharitdet 1918). Nan occupied the second location for only a decade and was forced to move to the next location Ban Huay Khrai (Ban = village in Thai) in AD 1368 due to water shortage (Ongsakul 1996). This third location, on the opposing site of the river, was called Wiang Tai (Wiang = city, Tai = south) and was occupied for more than 400 years (AD 1368–1818). Nan city needed to be relocated to a fourth location due to a flood catastrophe in AD 1818. According to local scripts, the flood destroyed the entire city when the Nan River changed its direction (Ongsakul 1996; Pharitdet 1918; Thongngern et al. 2007). The fourth location was called “Wiang Nuea” (Nuea = north) and was located northeast of the third location but was abandoned after only 35 years. Eventually, Nan was relocated to the same area as the third location in AD 1854, being called “Wiang Nan”. Even though this area was resettled, it is counted as a new city location in the historical papers (Pharitdet 1918). This fifth location comprises the old town of Nan until the present.

The first documentation of an ancient Nan city wall was during the reign of King Phra Ya Nguan Lar Phasum (AD 1426–1433). The king apparently demanded the construction of the wall, which was built over a period of eight years (Ongsakul 1996). According to a report of the Fine Arts Department (2012), inferred from scripts of the Phra That Chang Kham Temple, the wall was built as a log stockade.

The second time a historical paper indicates the presence of a city wall was during the reign of King Inthakanthao (AD 1435–1450), who fought with his two brothers over the throne. The paper describes an elephant duel (individual combat on an elephant's back) of King Inthakanthao with one of his brothers. The king came from outside and rode the elephant across the Nan River to fight with his brother on the city side (Ongsakul 1996). A report of the Fine Arts Department (2012) points out that what currently is known as Sumon Thewarat Road (STR; Fig. 1B) was the location of a former channel of the Nan River during that time. This context implies that the Nan River was functioning as a moat in addition to the log stockade city wall that remained from the previous reign (Fine Arts Department 2012).

The third mentioning of a city wall refers to the time when Nan fell victim to external political problems and lost the war to King Tilokaraj of Chiang Mai, becoming a dependency of the Lanna Kingdom in AD 1450. In this war, Chiang Mai troops used cannons to shoot from the Suan Tan Temple (Fig. 1B) through the city gate, and into the city area (Ongsakul 2005; Paritdet 1918).

A further mentioning of a city wall in Nan is linked to the reign of King Chao Phara Ya Muang Raja (AD 1689–1703). Nan had been under Burmese suzerainty from AD 1558 (Burma War I) and attempted liberation. Burmese troops attacked Nan city in AD 1703 (Burma War II) and burned it down while the king escaped. The city wall was severely destroyed and the city was abandoned for five years (Ongsakul 1996). Nan was resettled during the reign of Chao Fah

Mueang Kong (AD 1708–1714) while still under Burmese suzerainty.

The fifth mentioning of the Nan city wall in historical documents refers to the reign of King Ananta Worariththi Det (AD 1855–1891). Since AD 1800, Nan was under Siamese suzerainty and King Ananta Worariththi asked permission from King Rama IV of Siam to relocate the city from Wiang Neau (4th location) to the south, to the previous location of Wiang Tai (5th location; Pharitdet 1918). This last relocation was finalised in AD 1857 and entailed the construction of a new city wall (Thongngern et al. 2007). This wall is assumed to be depicted on the wall paintings at Si Phan Ton Temple in Nan that still can behold (SI Fig. A).

Site description

The present city of Nan is located in north-eastern Thailand on the floodplain of the Nan River with the Phi Pan Nam mountain range to the west and the Luang Prabang to the east. These ranges strike from north to south, embracing an intramountainous basin that gives space to the floodplain of the Nan River. Altitudes of the entire Nan region range between 200–2041 m above mean sea level (all elevation data reported here is referring to mean sea level). The Nan River flows from north to south through the basin with a meandering single channel that is sourced in the Luang Prabang mountain range to the north close to Pua (Fig. 1).

When comparing an aerial photo from AD 1954 with the most recent satellite image from AD 2021 (Google Earth 2021), it becomes apparent that the city of Nan used to have an asymmetric shape, influenced by the path of the Nan River, and was surrounded by moats, one of which likely was a former channel of the Nan River (Fig. 1). In contrast to other cities in Lanna, such as Chiang Mai which adopted a square shape (e.g. Srinurak and Mishima 2017), Nan kept its asymmetrical shape. Possibly, a city wall was constructed on top of a riverbank, similar to other places in the former Lanna Kingdom, such as Chiang Saen (Wood et al. 2015).

While notable, the preceding discussion regarding the shape of Nan city is difficult to further investigate due to a lack of reference archaeological sites and the subsequent extension of modern settlements. Today, only the MHW and PWT sites preserve ancient wall structures and remnant moats in the old town area of Nan. Parts of the wall at the MHW site (Fig. 1B) were demolished to build the Si Mueng Park and the Krungsri Bridge (Nokngam 2018). The Fine Arts Department (2012) assumes that the wall and moat at the PWT site continued northwards towards the area of the present Nan bus terminal. It is expected that Nan might have had two moats encircling the city (Fine Arts Department 2012). However, the traces of moats are puzzling, and it is hard to identify the connection to when the area was resettled.

The remains of the city wall along Mahawong Road (Fig. 1B; MHW) are composed of brownish to orange bricks. The wall is 6 m high, 5 m wide and is located on a one-meter-tall earthwork foundation. An octagon building with a roof acting as a watch tower is located at the junction of Anata Worariththi Det and Mahawong Road (Fig. B in SI). A moat of about 8 m width runs parallel along the wall. The wall is divided into two fragments by the Mahawong Road (Alley 1), at a location which is assumed to have been a city gate. Evidence from seven test pits (1.5 × 1.5 m to 3 × 3 m) examined to understand the foundation of the city wall revealed it was built on a broken brick compression, which might be remains from an older wall (Fine Arts Department 1993). Furthermore, several clay tiles, copper bullets, and pieces of pottery were found). The pottery originates both from local and regional production but also comprises pieces assigned to the Ming Dynasty of China (AD 1368–1644). From the age of the pottery, it has been assumed the city wall might date between the thirteenth-seventeenth century AD (Fine Arts Department 1993).

The other remainders of an ancient wall are located in the south-west of the city area and are preserved as an earthwork with moat in the area of Phaya Wat Temple (PWT). The earthwork is 6 m high, ca. 20 m wide. No brick structure is present at the surface and only individual bricks, which are assumed to have formed the foundation of the wall, remain on the surface. On top of the wall, today several trees grow, such as giant tamarin and bamboo. Outside of the wall is a moat which is currently used as a seasonal canal. There are no structures or traces of excavated overburden in the area. From this, it is assumed that sediment was dredged from the moat and placed on the brick structure. An excavation of the wall's earthwork by the Fine Arts Department (2012) unveiled a brick structure underneath the earthwork. In total, eight pits were excavated to understand the structure of the wall, inspect cultural aspects, and try to deduce past human behaviour. The wall previously extended in NW to SE direction, but parts were destroyed by recent settlements. However, it is assumed that the wall ended at Nan River (Fine Arts Department 2012). The location of the end point is inferred from the remains of an apparent earthwork structure and the AD 1954 aerial photo. From the archaeological point of view, the wall structure has been assumedly built on top of the earthwork and continued as a long trench. Due to roadworks in the AD 1960s, the wall was cut during construction of a small road leading to a primary school, now the location of Nan Primary Education Service Office (Fig. 1B and Fig. 3A). The construction of the earthwork is assumed have taken place during the thirteenth-seventeenth century AD due to the pattern of the pagoda at the PWT (Fig. C in SI), and pottery fragments found during excavations (Fine Arts Department 2012). These obtained 954 pieces of pottery (earthenwares, stonewares, and porcelains), which according

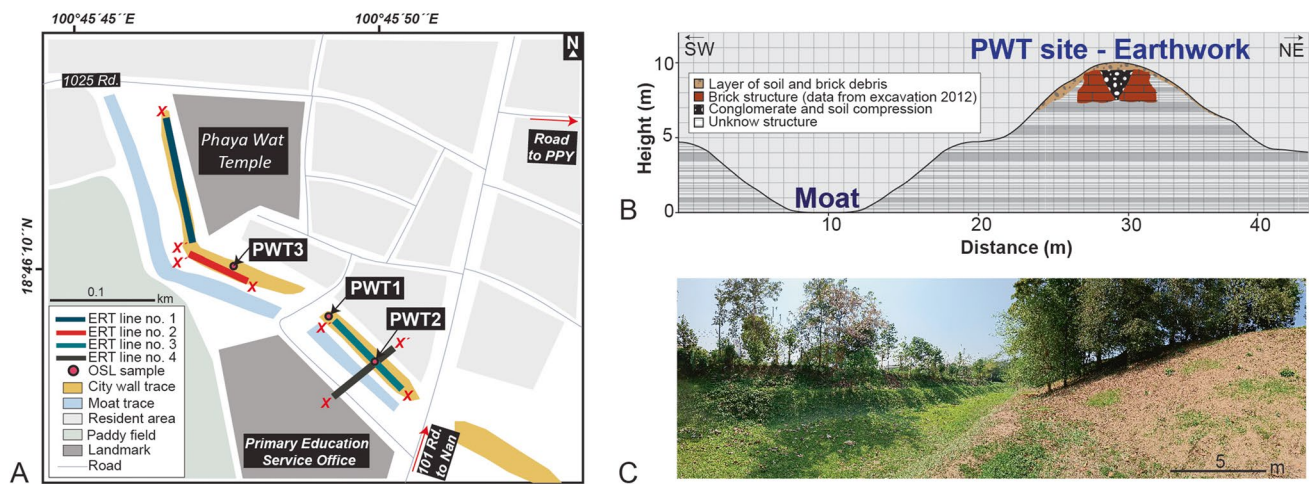


Fig. 3 **A** Map showing the location of ERT survey lines at the PWT site (x marks the begin and x' the end of the survey line). Also indicated are locations for OSL sampling. **B** Sketch of the cross section of the moat and earthwork at PWT. The location of the brick structure is

indicated as derived from the excavation of the Fine Arts Department (2012). **C** Photo of the earthwork and moat at the PWT site, facing NW, taken in March 2022

to their typology are pieces from local kilns in Nan (Ban Bo Suak), and other sites in Thailand such as Phra Yao (Mon Aom) and Sukhothai (Ko Noi). In addition, pottery from China assigned to the Ming Dynasty (AD 1368–1644) and the Qing Dynasty (AD 1644–1911) were found. It must be pointed out that the age of the pottery derives from stylistic analysis. Interestingly, the pottery represents a rather wide chronological span. Possibly, this pottery might have been discarded as litter making it difficult to exactly determine the age of this site based on the pottery alone (Adams 2003).

During sampling, we observed that the found bricks vary in size and colour and reveal differences regarding the amount of rice husks used during production. According to Mr. Phonphayuha Chaiyarot, an archaeologist from the Fine Arts Department, bricks were considered a tribute to the king in the past. Therefore, bricks likely came from several villages that used different sources and rice-husk-to-sediment ratios.

Production of bricks

Today, traditional handmade brick factories are found in the village Ban Phuang Pha Yom (PPY) to the west of the Nan River (Fig. 1B). Each local factory is a family business and brick making is mostly a side job for farmers from January to May, which is the dry period with insufficient availability of water to start crop plantation (mainly rice). Aerial photos (Fig. 1A) show that the factories were reached by a meander of the Nan River in AD 1954. According to interviews with local people, the brick factories have been in this area for more than 200 years, and the owners generally inherited the businesses from their parents. The bricks from PPY

contain three major elements, clay from termite mounts, rice husks, and coarse sand. Local brick makers still use a traditional technology to make bricks by first mixing these three components. Then, in the moulding process, the mixture is solidified in a rectangle form (not more than 5 cm thick). The still soft bricks are dried in the sun afterwards. Finally, the bricks are fired at high temperature (around 600 °C) in a brick firing place over open flames for 24 h (Fig. D in SI).

The function of rice husk in the mixture is to decrease the compressive strength, lower the bulk density, and increase the porosity of the brick as it also burns during the firing process and creates pores (Sutas et al. 2012). However, the rice husks also help to absorb moisture from the clay, which speeds up the moulding and sun drying processes. Another factor of using rice husks is the availability of the material. Wet rice cultivation was the main source of income for the ancient cities of northern Thailand and rice husks are a by-product of the rice polishing process (Janbuala and Wasanapiarnpong 2015; Lertrit 2000).

From the PPY site observations, it is shown that traditional brick production is still practiced in the region and likely utilizes the same primary components as were used for the ancient bricks from the city walls (clay, sand, and rice husk). However, a notable distinction is that the modern bricks (Fig. D in SI) are of reddish yellow colour (5YR 7/6 in Munsell's soil colour system), whereas the MHW site bricks are yellowish red (5YR 5/8). However, bricks from both sites show the same colour on the inside and outside. The bricks from the PWT site are light reddish brown (5YR 6/3), with a core of grey colour (5YR 5/1). All the bricks from the three sites exhibited a rough and porous texture due to the inhomogeneous mixture of materials. The PPY bricks

had the most porous texture, with visible coarse sand grains. The MHW site's bricks had a smoother texture than the other two sites, possibly due to the finer material used. The matrix was homogenous but showed obvious traces of rice husks, which reduced the number of pores in the bricks. In contrast, the bricks from the PWT site had a coarse texture due to the use of coarser material and a high number of pores, which may have resulted from the burning of rice husks and other organic material involved in the mixture process. We measured the bulk density of bricks from each site which results in a wide range from 1.3–2.5 g/cm³ (PPY 2.2 g/cm³, MHW 1.6–2.1 g/cm³, PWT 1.3–2.5 g/cm³).

Methods

Geophysical survey

The wall's internal structure and superposition to the subsequent sedimentary deposits have been non-destructively analysed by several ERT profiles. The ERT can help to constrain the archaeological interpretation, particularly for sediment-buried structures such as walls or ditches (Negri et al. 2008; Osella et al. 2005; Verdonck et al. 2019; Wunderlich et al. 2018).

ERT lines were acquired with a ABEM resistivity meter (Terrameter SAS 4000). In order to retrieve a tomographic reconstruction, the two-dimensional systems are capable of handling automatic protocols for data acquisition in which current and potential electrodes are automatically switched as channels along the surveyed line. The Terrameter SAS 4000 can connect up to 42 channels with two cables in one multi-electrode array. Five 40 to 90 m long ERT survey lines have been conducted, using a dipole–dipole configuration, of which ERT Line no. 1–4 use a spacing of steel rods used as electrodes of 1.5 m. In addition to Line no. 4, being located across the moat and wall, we made a sub profile along Line no. 4 only crossing the wall with an electrode spacing of 1 m (Fig. 3). The electrode locations were referenced with a DGPS and by total station theodolite, where foliage inhibited the DGPS signal. The collected ERT data is then filtered for electrodes with bad ground coupling. After exclusion of those data points, inversion of the data was performed with Res2DInv from Aarhus GeoSoftware.

Luminescence dating

Luminescence dating techniques enable the determination of the time elapsed since mineral grains were formed, last exposed to daylight, or heated to temperatures of several hundred degrees Celsius (e.g. Jacobs and Roberts 2008; Preusser et al. 2008; Liritzis et al. 2013). When exposed to light or heat, the luminescence signal stored within mineral

grains is erased, either optically or thermally, until it is entirely depleted (zeroed). Once the grains are shielded from sunlight and maintained at ambient temperatures, the luminescence signal gradually builds up again, stimulated by naturally occurring radioactivity. By dividing the accumulated signal by the dose rate, a brick production age can be determined. As bricks are usually made for a specific purpose, it is considered the production age reflects the building time of a structures (construction event). However, age overestimation of the time of construction may occur if bricks are reused from older structures (e.g. Alves and Sanjurjo-Sánchez 2015; Blain 2010), and age underestimation can be caused if bricks are added to a structure that have been manufactured specifically for later renovation works (e.g. Moropoulou et al. 2018; Pailoplee et al. 2016).

Sampling

Samples were collected in March 2022 from the PPY brick factory and at the MHW and PWT sites, totalling 12 bricks (Fig. 1B). A modern brick (PPY) was taken to investigate conceptual issues related to dating, i.e., the intensity of OSL signal, as observed for nearby kilns (Srisunthon et al. 2022). According to the factory owner, his bricks are composed of rice husk, local coarse sand, and clay from termite mounds that was brought in from another area. Rice husks contribute about 5% to the brick weight. The modern brick was 24 cm wide, 11 cm high, and 5 cm thick and dried in a brick firing place for 24 h between March 29th–30th, 2022.

Two locations were selected at the MHW site: MHW1 on the east side of Mahawong Road and MHW2 on the west side (Fig. 1A). This section is exposed since its construction as it was the site of a city gate, “Suan Tan gate” constructed before the modern settlement built the road of Mahawong alley 1 in between (Fine Arts Department 2012). Sampling was conducted on exposed walls at both sides of a roadside cutting at an elevation of 203 ± 14 m (Fig. E in SI). Before sampling, the wall was cleaned from vegetation overgrowth. While the bricks of the wall were of similar appearance, we found traces of grouting (about 1 cm thick) between the bricks. Bricks were collected at heights of 118 cm (MHW1#1), 114 cm (MHW1#2) (Fig. 4A), 142 cm (MHW2#1), and 140 cm (MHW2#2) (Fig. 4B).

For sampling at the PWT site, three locations (PWT1, PWT2 and PWT3) were selected (Fig. 1B and 3A). PWT1 is an exposed cross-section of the wall at a roadside cutting from AD 1960s and sampling was conducted at road level (206 ± 10 m). Sediment covering the bricks was about 5 cm thick homogeneous clay-sand (colour 7.5 YR 5/6). Those bricks appear to have slipped from the top. We opened a 60 cm wide and 140 cm high profile to collect two bricks at heights of 70 and 100 cm (Fig. 4C). PWT2 is located at the top of the earthen wall (210 ± 10 m). The sediment covering

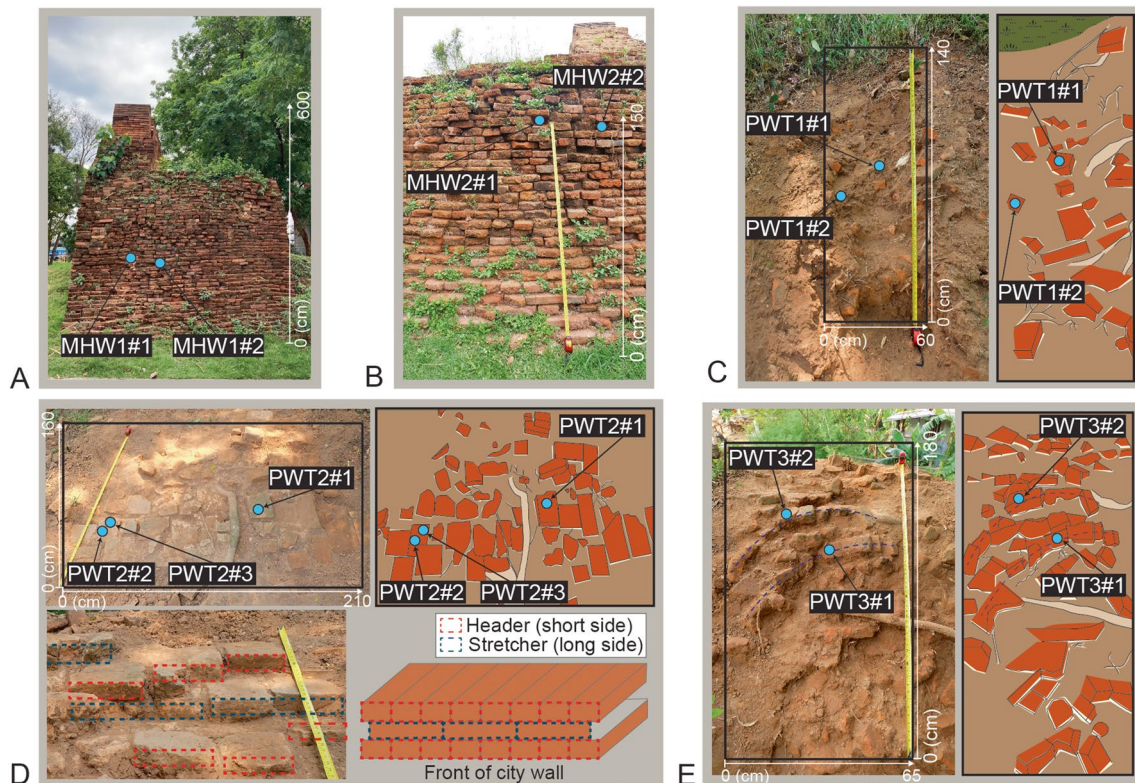


Fig. 4 Sampling locations at the ancient city walls. **A** Photo of location MHW1. **B** Photo of location MHW2. Photo and sketch of profile PWT1 (**C**), PWT2 (**D**), and PWT3 (**E**)

the bricks is clay-sand (colour 5YR 5/6), about 5 cm thick that was cleaned off. At this location, the bricks seem to have a systematic arrangement (pattern), with rectangular bricks organised in layers. Alternating rows of bricks were laid with either the long sides facing outwards (stretchers) or the short sides facing out (headers). This brick arrangement reminiscent of the current English bond in brick masonry. We opened a 210 cm wide and 160 cm long profile along the apex and downward slope of the earthen wall. Three bricks were collected between 20–50 cm from the bottom of the profile (Fig. 4D and Fig. F in SI). PWT3 is also located on the top of the earthen wall (210 ± 10 m), further to the NE in the backyard of the Phaya Wat Temple (Fig. 3). The sediment covering the bricks is ca. 5 cm thick homogeneous clay-sand (colour 5YR 5/6). Because of the degradation of the wall on the temple side, determination of a brick pattern was prevented albeit it is known to have been preserved at this side from the Fine Arts Department report (2012). The bricks at PWT3 vary in size but are generally smaller than at the PWT2 location. We opened a 65 cm wide and 180 cm long profile on the apex of the earthen structure to collect two bricks with at 90 and 105 cm (Fig. 4E). Note that for all bricks from PWT site, we collected the surrounding sediment of each brick for later dose rate determination.

Sample preparation

All brick samples were prepared following these five steps: (1) cutting and subsampling, (2) removing the light-exposed surface, (3) crushing, (4) chemical treatment, and (5) retrieving the desired grain size by sieving. All preparation processes were carried out under subdued red-light conditions to preserve the luminescence signal. The preparation began by cutting the bricks with a saw equipped with a diamond blade to obtain three subsamples, except for samples PWT1#1 and PWT3#1 where only two samples were obtained due to the limited size of the bricks. During the cutting, the blade was water-lubricated to avoid any loss of luminescence signal due to excessive heating. The modern brick (PPY) was divided into a left (L), middle (M) and right (R) part using the long side as reference point. This concept was also applied for each brick from the PWT site as all bricks were from a stretcher layer with the long side pointing outwards of the wall structure (Fig. F in SI). However, for the MHW site the location of the individual subsamples in relation to the wall structure had to be defined. Subsamples were labelled inner (i), middle (m) and outer (o) in regards to their position on the wall (Fig. E in SI). This is important for determining the dose rate as the position determines the

amount of cosmogenic radiation and dose from surrounding material that each subsample has been exposed to.

Following this procedure, a total of 34 subsamples were prepared and used for OSL measurements to provide an individual age for each subsample. After cutting, about 1 cm of the brick surface was removed since it was exposed to light, and only the brick core was further processed for OSL measurement. Each subsample was dried at 50 °C in the oven overnight. The subsamples were gently crushed using a mortar and were sieved to <2 mm. Since the samples are clay-rich, they were first rinsed with water before chemical treatment to avoid heavy reactions. Then, they were etched in 40% hydrofluoric acid for 60 min to remove the outer surfaces of the quartz grain and purify the quartz by dissolve unwanted feldspar grains. Subsequently a 20% hydrochloric acid treatment was used for 60 min to remove residual fluoride. Grains of 63–200 µm were eventually extracted in the last stage by dry sieving. For each measurement, we used a 6 mm diameter aliquot or ca. 1350 grains of coarse quartz. The grains were adhered to stainless-steel discs using silicone oil.

Equivalent dose (D_e) measurement

A Risø reader (TL/OSL-DA-15C/D) was used to measure the OSL or equivalent dose (D_e). The device is fitted with a beta source ($^{90}\text{Sr}/^{90}\text{Y}$) with a dose rate of ca. 0.10 Gy s⁻¹ for laboratory irradiation, a blue LED (470 nm) stimulation

light unit, and a photomultiplier tube That has a Hoya U-340 UV filter with a thickness of 7.5 mm is positioned in front it. For each measurement, only 24 discs were placed on the 48-position carousel to avoid cross-talk between the discs (cf. Bray et al. 2002).

We followed the single-aliquot regenerative dose (SAR; Murray and Wintle 2000) protocol using constant LED power to obtain the continuous wave OSL signals. For all PWT samples, a normal SAR protocol was used (here called SAR1), while for samples from MHW and PPY, a SAR protocol (SAR2) was used in which regenerative dose points are measured twice to improve the fitting of the dose response curve in the presence of low OSL signals (poor counting statistics).

Sample PWT2#2L was selected to carry out performance tests (preheat plateau, thermal transfer, and dose recovery tests; cf. Wintle and Murray 2006) D_e measurement. Preheat temperatures of 180 °C, 200 °C and 220 °C were tested to identify the effects of thermal treatment. The preheat plateau test was performed on the natural signal for ten aliquots following the SAR1 protocol (Table 1). For the dose recovery test, five aliquots were measured per temperature after erasing the natural signal using blue LEDs and then giving a regenerative dose of 0.95 Gy. Thermal transfer tests are especially crucial for young samples since preheating may increase the apparent dose absorbed since the production of bricks, i.e., the time to be dated (Rhodes 2000; Wintle and Murray 2006). This test

Table 1 Overview of the of the protocol used for D_e determination

Protocol	Step	Operation
SAR1 ^a	1 ^b	Irradiation; given regenerative doses are 0.95, 0.48, 1.90, 0 and 0.95 Gy
	2	Preheat of 200 °C for 10 s
	3 ^c	Infrared stimulated luminescence (IRSL) measurements 40 s at 0 °C
	4	Optical stimulation for 60 s at 125 °C (L_x)
	5	Irradiation; test dose of 0.86 Gy
	6	Preheat of 160 °C for 10 s
	7	Optical stimulation for 60 s at 125 °C (T_x)
	8	Repeat step 1–7 with the other regenerative doses
SAR2 ^d	1 ^b	Irradiation; given regenerative doses are 0.19, 0.38, 0.57, 0, 0.19, 0.38, 0.57, 0 and 0.19 Gy
	2	Preheat of 200 °C for 10 s
	3 ^c	Infrared stimulated luminescence (IRSL) measurements 40 s at 0 °C
	4	Optical stimulation for 60 s at 125 °C (L_x)
	5	Irradiation; test dose of 0.86 Gy
	6	Preheat of 160 °C for 10 s
	7	Optical stimulation for 60 s at 125 °C (T_x)
	8	Repeat step 1–7 with the other regenerative doses

^aThe standard SAR protocol was only used for samples from the PWT site

^bOmitted during the first SAR cycle (measurement of the natural signal)

^cOnly performed for the last SAR cycle of the measurement

^dThe repetitive SAR protocol was used for sample from the MHW and the PPY site

was also conducted for five aliquots at each temperature. In addition, dose recovery and thermal transfer tests with a 200 °C preheat temperature were performed on samples MHW1#2 m and PPY1#1R.

Individual D_e values were obtained using the first 0.4 s of the OSL signal with a background reduction using the last 10 s. Aliquots were rejected if they passed one of the following criteria: (1) recycling ratio outside 10% of unity, (2) test-dose signal error > 20%, (3) weak test-dose signal (T_n) with an intensity of below 3σ of background, (4) failure to fit the dose response curve with the fitting function, (5) non-identical decay curves of the natural and first regenerative dose signal (Fig. G in SI). The number of rejected aliquots with these criteria is presented in Table H in the SI. The Central Age Model (CAM) of Galbraith et al. (1999) was applied to derive weighted mean values using the R luminescence package (Kreutzer et al. 2012). One factor to be considered before calculating mean D_e values using the CAM are outliers. The normalised median absolute deviation (nMAD) was applied as statistical method to detect and reject outliers in each sample (Powell et al. 2002). In this case, 1.4826 was used as the correction factor for the normal distribution and each D_e value which was greater than 1.5 was rejected.

Dose rate measurement

The content of radioactive elements in the bricks and sediment was measured using high-resolution gamma spectrometry (HRGS). For the bricks, the remaining parts after subsampling were dried and crushed using a mortar to obtain a grain size below 2 mm; 150 g were collected per sample. Sediment samples were prepared accordingly. After preparation, the samples were placed in air-tight plastic containers for a month to allow radon to accumulate. All samples were measured at VKTA laboratory (Dresden, Germany) and results are presented in Table 2. There is no evidence for the radioactive disequilibrium (cf. Degering and Degering 2020) in any of the samples.

In archaeological contexts, dose rate calculation can be complex due to inhomogeneous settings (cf. Degering and Degering 2020; Schwarcz 1994). In the present case, this in particular refers to the amount of radiation emitted from a brick in comparison to the surrounding mixture of sediment and brick fragments or air. We considered this using the layer model available in ADELE software (Degering and Degering 2019), which allows to calculate dose rate for three different layers (A, L and B) of different radioactive element content. For this study, we use A and B as layers

Table 2 For dose rate determination, radioactive element and water contents were determined. Field water (W_f) was measured after sample collection, short-term (W_{60}) and long-term (W_{Sat}) water uptake capacities were obtained experimentally. For further details see “Assessment of brick water content”

Site	Sample name	Sample	Bulk density (g/cm ³)	Water content (%)			Radioactive element content		
				W_f	W_{60}	W_{Sat}	U (ppm)	Th (ppm)	K (%)
PPY	1#1	Brick	2.20	6	22	25	2.80±0.50	10.70±0.70	0.61±0.05
MHW	1#1	Brick	1.90	17	24	26	3.10±0.40	11.00±0.70	1.90±0.12
	1#2	Brick	1.60	13	24	27	2.50±0.40	9.80±0.60	1.55±0.10
	2#1	Brick	2.00	29	29	33	3.10±0.40	9.80±0.60	1.58±0.11
	2#2	Brick	2.10	15	22	25	2.10±0.30	7.30±0.50	0.67±0.05
	DR-MHW2-1	Grouting	-	5	-	-	1.30±0.26	4.40±0.30	0.63±0.06
	DR-MHW1-1	Grouting	-	1	-	-	1.50±0.40	4.00±0.30	0.53±0.07
PWT	DR-MHW1-1	Brick	-	19	23	26	2.70±0.40	9.20±0.60	1.60±0.11
	1#1	Brick	2.20	19	23	26	2.60±0.30	10.20±0.70	1.41±0.12
	1#2	Brick	1.70	20	25	24	2.60±0.30	9.90±0.60	1.17±0.08
	2#1	Brick	2.10	13	16	17	2.34±0.29	8.00±0.50	0.69±0.07
	2#2	Brick	1.60	8	18	22	3.00±0.40	9.50±0.60	1.42±0.12
	2#3	Brick	2.50	12	18	21	2.20±0.30	7.80±0.50	0.61±0.04
	3#1	Brick	1.40	20	19	22	3.30±0.40	10.70±0.70	1.52±0.16
	3#2	Brick	1.90	24	27	^a	2.70±0.30	9.50±0.60	1.03±0.09
	DR-PWT1-1	Sediment	-	10	-	-	2.80±0.30	9.10±0.60	1.34±0.14
	DR-PWT1-2	Sediment	-	10	-	-	2.70±0.30	9.30±0.60	1.42±0.12
	DR-PWT2-1	Sediment	-	8	-	-	2.10±0.30	7.50±0.50	1.07±0.07
	DR-PWT2-2	Sediment	-	7	-	-	2.30±0.30	7.70±0.50	1.03±0.11
	DR-PWT2-3	Sediment	-	13	-	-	2.70±0.30	7.50±0.50	1.02±0.09
DR-PWT3-1	Sediment	-	13	-	-	2.50±0.30	8.50±0.60	1.18±0.08	
DR-PWT3-2	Sediment	-	19	-	-	2.70±0.30	9.00±0.60	1.23±0.13	

^aMaterial was lost after five days of soaking in water

for the surrounding and the L layer for the brick at the PWT site. For the MHW site, the A layer is used to account for the limited horizontal extent of the wall (an air layer with zero radioactive concentration), whereas the L and B layer represent bricks. The grouting between the bricks was neglected as it was too thin (less than 1 cm) to create a significant effect in dose rate. We calculated the ages using the bulk density (g/cm^3) following the data from Table 2. All dose rates and ages were calculated using ADELE v2017 software (Degering and Degering 2019).

Assessment of brick water content

Water content in the pores causes an attenuation of the effective dose rate but is difficult to be securely estimated for longer periods. In particular in tropical monsoon areas, the water content between the wet/dry period differs considerably. Therefore, measurements of present-day water content might not be representative for the time since the event to be dated; a too low water content will cause overestimation of the dose rate and underestimation of the real age (Costas et al. 2012). This problem is approached by using estimated water content for long-term conditions, for example by modelling using grain-size characteristics (e.g. Nelson and Ritzenour 2015; Wood et al. 2016).

Initially, all bricks and sediment samples were dried and field water content was determined (Table 2). The bricks of this study were sampled in March 2022, which was abnormally wet for the season (ca. 136% precipitation above average, Thai Meteorological Department 2022). Hence, in situ the water content might overestimate the true average. To

examine this issue, the saturation water content was measured following Bailiff (2007) by immersing dried pieces cut from the bricks in 500 ml water at room temperature for 60 min and then determining the weight difference. This allows to estimate the water content uptake over a short period of time (W_{60}). Subsequently, the same pieces of bricks were immersing as in the previous step but left for five days to measure the saturation water content (W_{Sat}). The results are presented in Table 2 and discussed below.

Results

ERT results and inversion

Three of the five acquired ERT profiles were collected along a footpath on top of the city wall. The northern most being ERT profile no.1, directly next to the Phaya Wat temple, and profile no.4 extending furthest to the south. Since foliage inhibited the DGPR here, the elevation of electrode locations was determined by total station measurements.

Figure 5 shows three stacked profiles showing the inversion model results from the field ERT measurements in Res2DInv. The top profile shows measured apparent resistivities, while the middle one displays calculated values derived from a model with actual subsurface resistivities obtained through inversion of measured data, allowing a visual comparison between the measured and calculated apparent resistivity profiles to assess the fit of the inversion model. This fit of the inversion model is quantified by the Root-mean-square deviation (RMS), here 6.18%. For profile lines no. 1–4,

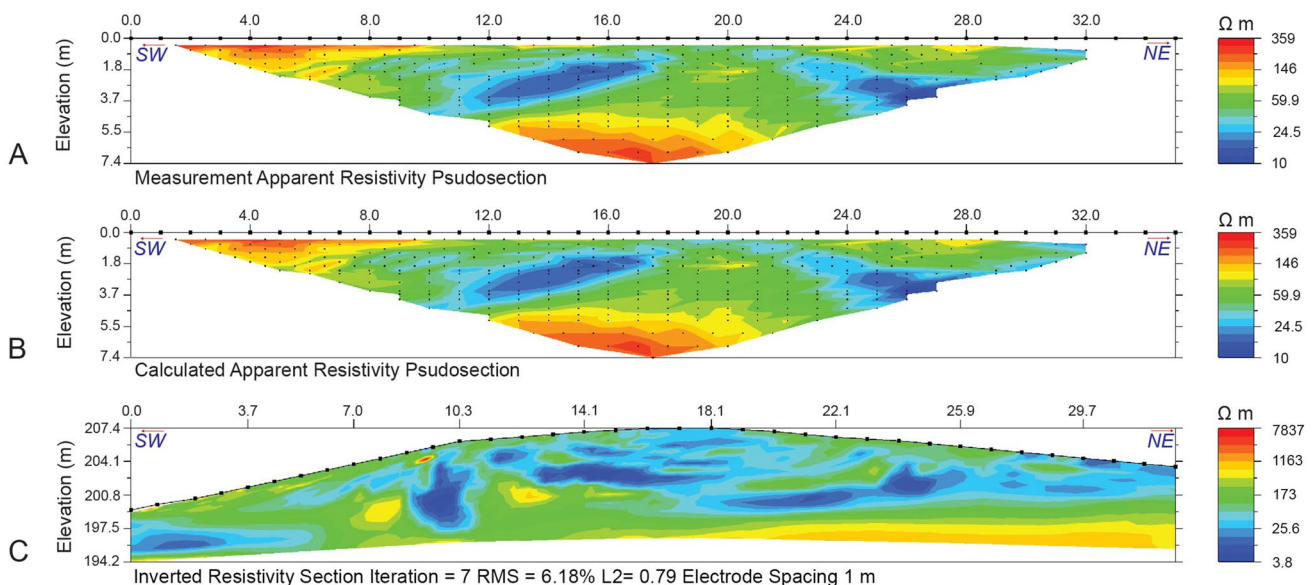


Fig. 5 ERT Line no.5 from SW to NE, starting SW. **A** The measured apparent resistivities. **B** Calculated apparent resistivities which derived from **C** the inversion modelled subsurface resistivities displayed last. Black dots indicate individual measurements and their representative depth

measured and calculated apparent resistivity profiles can be found in the appendix and only the RMS is provided here to assess the fit of the inversion model.

Line no.1 exhibits low to moderate resistivity in the inversion (~ 10 to $400 \Omega \text{ m}$), indicating high overall subsurface conductivity (a). The profile reveals a very shallow uppermost layer approximately one meter thick, with intermittent interruptions along the profile. Cobbled bricks atop the wall are visible, occasionally disrupted by trenches, trees, and ditches, correlating with interruptions in the uppermost layer, notably a ditch from 97 to 107 m. Higher resistivities in the shallow layer are thus linked to sections of intact open brick construction, compared to remodelled or excavated sections. A slightly sloped initial section appears visually more reworked (b). A subsurface domain (50 to $200 \Omega \text{ m}$) with varying thickness is identified, extending laterally up to 50 m. This domain transitions laterally into a section with lower resistivities (as low as $10 \Omega \text{ m}$), interspersed with sub-vertical patches of relatively higher resistivities (c). Along this part, trees, trenches, and moats are present, primarily

in the mid-to-southern section. The sloped section suggests potential internal structural differences, indicative of material changes or subsequent remodelling mostly in the mid-to southern-section.

Line no. 2, collected in a 60 m short array (Fig. 6A), shares similarities with Line no. 1, featuring a shallow uppermost layer (up to 1 m thick) with consistent lateral continuity (a). Beneath, resistivity distributions show greater lateral homogeneity (c), ranging from a few tens to $100 \Omega \text{ m}$.

ERT Line no. 3, spanning 90 m with two overlapping arrays (Fig. 6B), intersects cross-cutting profiles at 37 m. This profile exhibits elevated topography along the wall, with sections of higher resistivity in the upper layer (a) and a less contiguous lower resistivity domain (c) with 10 to $100 \Omega \text{ m}$. At 6 to 9 m depth, this domain (d) transitions to a higher resistivity horizon (several hundred to $900 \Omega \text{ m}$), with an unaccounted gap between 26.60 m and about 30 m attributed to the inversion method.

ERT Line no. 4, along an 80 m profile from a nearby parking lot, traverses moat and wall structures (Fig. 6C).

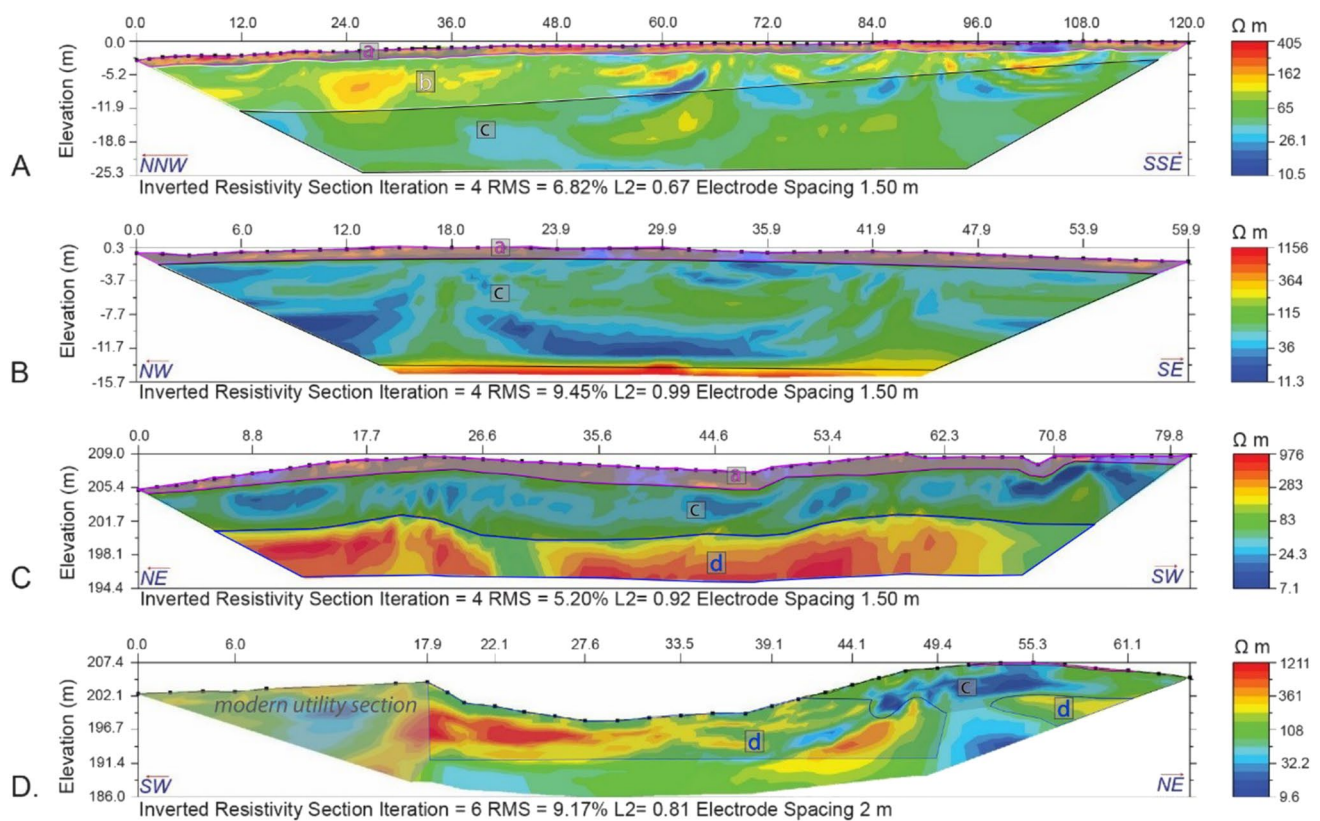


Fig. 6 ERT Lines no.1 to 4 with orientations from NNE-SSE to SW-NE, parallel and across the wall sections showing inversion of **A** ERT Line 1, **B** Inversion of ERT Line no.2 trending from NW to SE, starting NW. South of the sawmill adjacent to the temple. Elevation of electrode locations was determined by total station. **C** ERT Line no.3 from trending NE to SW, starting NE. Profile located on top of the south-eastern wall section, beginning at the 101 Rd. and ending

at the small city road cross cutting the wall. **D** ERT Line no.4 from trending SW to NE, starting SW. Profile crossing the moat and the wall at 37 m in Line no.3. The electrode locations for B and C are referenced by DGPS. Different identified resistivity domains are labelled A-D. The model fit-quality is indicated by the RMS shown below each individual profile

Ignoring the parking lot section, the profile reveals two distinct domains: a wall section in the NE with generally low resistivity (c) and a moat section in the centre with markedly higher resistivity characteristic from 100 to 1200 Ω m (d). The high resistivity moat section may be confined by a lower resistivity zone at an elevation of 190/192 m. The wall section displays a low resistivity domain up to seven meters deep, wedged by a similar higher resistivity zone from NE at 195 to 202 m.

Results of OSL dating

SAR protocol performance tests

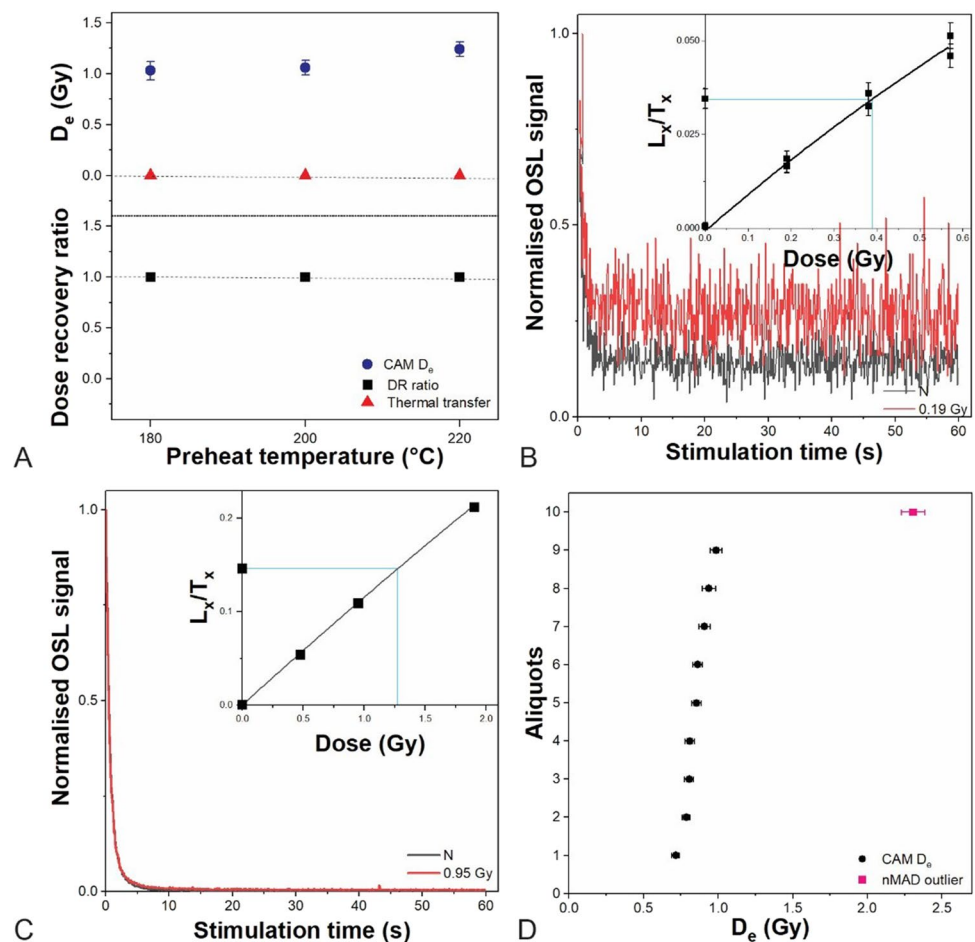
The results of the SAR OSL performance test using sample PWT2#2L are plotted for preheat temperatures of 180 °C, 200 °C, and 220 °C in Fig. 7A. The results of the preheat plateau test indicate a natural D_e plateau between 180 °C and 200 °C. For all preheat temperatures, dose recovery ratios are statistically consistent with unity and D_e values close to 0 Gy for the thermal transfer test indicate no significant transfer. Additionally, a good dose recovery and

negligible thermal transfer was found for a preheat temperature of 200 °C for samples PPY1#1R and MHW1#1 m. A preheat temperature of 200 °C was chosen and applied to all further measurement.

OSL signal and dose response curves

Examples of the normalised natural and regenerative OSL decay signals from the MHW and PWT site are given in Fig. 7B and C. The OSL signal of the sample from the MHW site presents a relatively dim signal with a high noise-to-background-ratio. However, the decay curve is dominated by the fast component and we observe an excellent reproducibility of the regenerative dose measurements. The signal intensities reach background level within 5 s. In comparison, the OSL signal from the PWT site shows bright decay curves dominated by the fast component. For each regenerative and the natural, the decay curve shapes were reproducible. The dose response curve, and the results from each regenerative dose point fit well using a single-saturating exponential function.

Fig. 7 Results of OSL performance tests. **A** The preheat plateau test ($n = 10$ for each temperature) shows a D_e plateau for all three tested temperatures. The thermal transfer test ($n = 5$ for each temperature) shows D_e values close to 0 Gy, indicating no thermal transfer effect. Dose recovery ratios ($n = 5$ for each temperature) are close to unity. **B** Example of typical OSL decay curves and a dose response curve (6 mm aliquot) of sample MHW2#1i. **C** Example of a typical OSL decay curve and dose response curve (6 mm aliquot) of sample PWT1#1L. Please note the much lower OSL signal in the first example but the excellent reproducibility of the regenerative dose points. **D** D_e values of sample PWT2#1R showing one upper outlier (in pink) which was rejected using normalised median absolute deviation (nMAD)



D_e values

For the modern brick sample (PPY), identical CAM D_e values of -0.04 ± 0.00 Gy were yielded from all three subsamples (Table 3). This highlights that all quartz grains received enough heat during the production process to fully reset the OSL signal. Similarly, the non-modern sample present only a small spread of D_e values, low overdispersion values, and a general consistency of mean D_e values (Table 3) indicating

fully reset signals during production. However, in some samples D_e outliers were observed that are significantly higher than the rest of the population (Fig. 7D). Such outliers were removed by nMAD, and the subsequent mean D_e values were used for age calculation (Table 3; shown as N_{cal}).

For the MHW site, CAM D_e values range from 0.16 ± 0.01 to 0.42 ± 0.02 Gy (Table 3 and Fig. 8). Subsample MHW1#1 shows the highest D_e value for the inner position of the sample, whereas samples from the middle and outer samples of

Table 3 Dose rate, D_e values and calculated ages

Site	Sample name	Dose rate ^a (Gy/ka)	N _{acc} ^b /N _{cal} ^c	CAM D _e (Gy)	OD ^d (%)	Age (a)	Age (AD) ^e
PPY	1#1L	-	10/10	-0.04 ± 0.00	0	-	-
	1#1 M	-	10/10	-0.04 ± 0.00	0	-	-
	1#1R	-	10/10	-0.04 ± 0.00	0	-	-
MHW	1#1i	2.88 ± 0.21	6/6	0.32 ± 0.02	16	111 ± 8	1900–1920
	1#1 m	2.77 ± 0.23	4/4	0.28 ± 0.02	0	101 ± 8	1910–1930
	1#1o	2.68 ± 0.22	10/10	0.28 ± 0.02	16	104 ± 9	1910–1930
	1#2i	2.38 ± 0.17	10/10	0.30 ± 0.02	13	126 ± 9	1890–1900
	1#2 m	2.31 ± 0.17	10/10	0.29 ± 0.02	4	126 ± 9	1890–1900
	1#2o	2.21 ± 0.12	10/10	0.32 ± 0.01	0	145 ± 8	1870–1890
	2#1i	2.58 ± 0.16	10/10	0.42 ± 0.02	11	163 ± 10	1850–1870
	2#1 m	2.36 ± 0.24	3/3	0.33 ± 0.03	0	140 ± 14	1870–1890
	2#1o	2.33 ± 0.12	10/10	0.34 ± 0.01	11	146 ± 8	1870–1890
	2#2i	1.45 ± 0.11	7/6	0.16 ± 0.01	15	110 ± 8	1900–1920
PWT	2#2 m	1.45 ± 0.13	11/9	0.25 ± 0.02	18	177 ± 16	1830–1860
	2#2o	1.35 ± 0.08	9/10	0.23 ± 0.12	13	171 ± 10	1840–1860
	1#1L	2.49 ± 0.11	10/10	1.25 ± 0.02	4	502 ± 22	1500–1540
	1#1R	2.50 ± 0.12	9/9	1.24 ± 0.03	6	497 ± 24	1500–1530
	1#2L	2.32 ± 0.09	10/10	1.15 ± 0.02	5	496 ± 19	1510–1550
	1#2 M	2.32 ± 0.09	10/10	1.13 ± 0.02	4	487 ± 19	1520–1540
	1#2R	2.23 ± 0.10	10/10	1.15 ± 0.03	8	496 ± 22	1500–1550
	2#1L	1.88 ± 0.12	10/10	0.96 ± 0.05	15	512 ± 33	1480–1520
	2#1 M	1.88 ± 0.09	10/8	0.83 ± 0.02	5	443 ± 21	1560–1600
	2#1R	1.87 ± 0.10	10/9	0.86 ± 0.03	9	464 ± 24	1540–1570
	2#2L	2.68 ± 0.13	10/9	1.00 ± 0.03	3	374 ± 19	1630–1670
	2#2 M	2.69 ± 0.22	10/10	1.14 ± 0.08	18	425 ± 34	1560–1600
	2#2R	2.67 ± 0.17	10/10	0.93 ± 0.05	14	348 ± 22	1650–1700
	2#3L	1.85 ± 0.09	10/9	0.85 ± 0.03	8	460 ± 23	1540–1570
	2#3 M	1.78 ± 0.08	10/10	1.02 ± 0.03	9	572 ± 26	1420–1480
	2#3R	1.80 ± 0.12	10/10	0.98 ± 0.08	25	518 ± 33	1460–1510
	3#1L	2.89 ± 0.14	10/10	1.33 ± 0.02	5	460 ± 22	1540–1590
	3#1R	2.86 ± 0.15	10/10	1.12 ± 0.03	7	392 ± 21	1610–1640
3#2L	2.34 ± 0.10	10/10	1.15 ± 0.02	5	492 ± 21	1510–1550	
3#2 M	2.34 ± 0.10	10/10	1.14 ± 0.02	4	488 ± 20	1510–1540	
3#2R	2.34 ± 0.10	10/10	1.07 ± 0.02	5	457 ± 19	1550–1580	

^aA longterm water content of $12 \pm 4\%$ was used. Please see “[Assessment of brick water content](#)” for further details

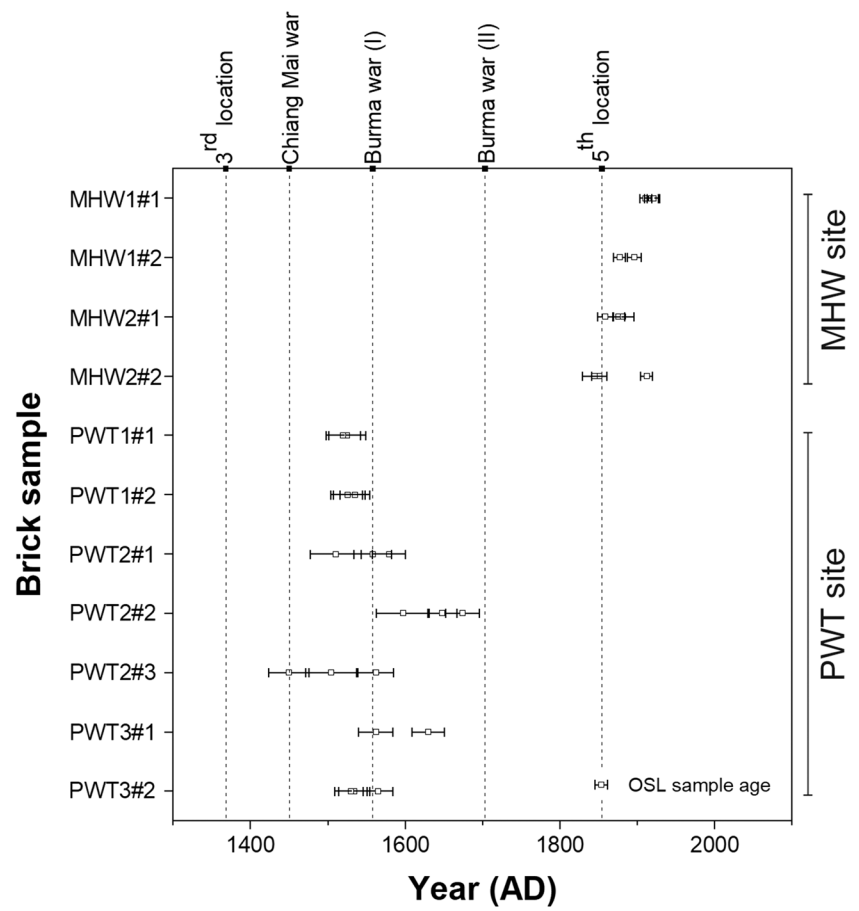
^bN_{acc} is the number of accepted aliquots

^cN_{cal} is the number accepted after outlier analysis (nMAD)

^dOverdispersion calculated using the CAM

^eAges in years AD were rounded to the next decade

Fig. 8 Summary of brick OSL ages. The ages of all individual subsamples are presented (indicated by black signatures). Additionally, the plot overlays significant events in Nan's history to identify potential correlations with the construction of the walls



the brick yield more or less similar D_e values. In contrast, the subsample MHW1#2 presents a different trend, with the inner and outer samples being almost identical and the lowest D_e value coming from the middle position. MHW2#1 and MHW2#2 show D_e values similar to MHW1#1, with the highest D_e value from the inner and the D_e value from the middle being close to the outer position.

For the PWT site, CAM D_e values range from 0.83 ± 0.02 to 1.33 ± 0.02 Gy which shows that the values are much higher than for the MHW site (Table 3 and Fig. 8). PWT1#1 and PWT1#2 show comparable D_e values for all sampling position. Subsample PWT2#1 and PWT3#1 have the highest D_e on the left position, but the other two subsamples are in good agreement. PWT2#2 and PWT2#3 show the highest D_e values at the middle position. Lastly, PWT3#2 has the highest D_e value at the right position.

Water content and dose rate values

The measured field water contents (W_f) of the bricks ranges from 8 to 29%, whereas the water uptake capacities after 60 min (W_{60}) and five days (W_{sat}) range from 16 to 29% and 17% to 33%, respectively (Table 2). Nevertheless, comparison of the data from the two experiments (mean values

$22 \pm 4\%$ and $24 \pm 4\%$) reveals that ca. 90% of the water saturation level in the bricks is reached already after 60 min. As results of the experiments are rather similar, we continue using data from the latter experiment in the following. This data reveals some variability in the water uptake potential ($\pm 20\%$ around the mean value), which is lower than the spread of values observed for the field water content (mean $17 \pm 6\%$, 35% variability). The field water content yields between 36 and 91% of the saturation level. This implies that the individual location of a brick in the landscape plays an important role, probably influenced by factors such as overburden thickness and brick nature as well as vegetation cover (type and size); of which the latter may have changed in the past. In addition, it has to be considered that the bricks were exceptionally wet during sampling and may dry out almost completely during the dry season. In the end, we assigned an estimated mean water content of $12 \pm 4\%$ in the dose rate determination, which reflects the mean between the possible extreme values (no water and saturation) and considers a high level of uncertainty (33%).

Total dose rates vary considerably with values between ca. 1.4 Gy ka^{-1} and almost 3 Gy ka^{-1} (Table 3). This range in dose rate is related to different contents of dose rate relevant elements, radionuclides, in the individual brick

samples (Table 2). For example, compared to brick MHW 1#1, brick MHW 2#2 contains only ca. 67% of U and Th, and only 35% of K. The significant variations in U, Th, and K values can be attributed to the dissimilar composition and structure of the bricks, possibly resulting from the use of different raw materials or manufacturing techniques among various brick makers or villages within the Nan province. As mentioned in Sect. 2.3, the primary components of the bricks are clay, sand, and rice husks, but the exact proportions remain unknown. Regarding the fabric, the smoother texture of some bricks suggests lower porosity, which could be attributed to the finer material used in their production. The different bulk density of bricks indicates different levels of porosity.

Age of the structures

OSL dating of the investigated bricks revealed that ages for the MHW wall site are significantly younger than those for the PWT site (Table 3 and Fig. 8). The city wall at the MHW site is between 101 ± 8 a (AD 1910–1930) to 177 ± 16 a (AD 1830–1860) years old. In contrast, the wall at the PWT site points towards a building age of between 348 ± 22 a (AD 1650–1700) and 572 ± 26 a (AD 1420–1480). It has to be noted that ages at the two sides do not all overlap within the given dating uncertainties (1σ) and is reflected by statistical parameters such as χ^2 and overdispersion (OD). For MHW ($n=12$), these are 82 (χ^2) and 17% (OD), whereas for PWT ($n=19$) values of 102 (χ^2) and 10% (OD) were determined. This could be explained in different ways.

While the usage of older bricks during construction or later replacement with recycled old bricks during renovation works is in principal possible, we observe partially large deviations with one particular brick, eliminating this as potential explanation. Hence, dose rate inhomogeneity is considered to more likely explain the observed scatter, i.e. the dose rate assumed for individual samples might not be fully appropriate. Interestingly, the MHW data set is almost equally distributed (low skewness of -0.43), whereas PWT is slightly more negatively distributed (skewness = -1.18) but shows a more narrow distribution (lower OD; 10% versus 17%). The most conservative approach is to use the entire range of ages including uncertainties to delimit the time of construction. This would result in age ranges of AD 1830–1930 (MHW) and AD 1420–1700 (PWT) but this approach will overemphasize extreme values. This is demonstrated by the fact that according to historic records, the construction of MHW only started after AD 1857 and it likely took several years to finish it. Hence, at least the lower 30% of the above estimated time range is not realistic. The arithmetic mean (\pm standard deviation) and CAM age for all MHW ages of 135 ± 26 a and 133 ± 7 a overlap within uncertainties and would further pin-down the time of construction to the late nineteenth century AD (AD 1860–1910 and AD 1880–1900, respectively),

which appears more realistic. Applying the same approach of eliminating extreme values to PWT results in consistent arithmetic mean and CAM ages of 468 ± 54 a and 466 ± 12 a, respectively (AD 1500–1610 and AD 1540–1570, respectively). This would indicate that construction of the PWT site likely occurred during the mid-sixteenth century AD.

Discussion

The low resistivity domains of a few tens of Ω m are found to be characteristic of the artificial earthen structure (resistivity domains a, b and c), which partly discontinues below 7–9 m depth. In the cross profile, the lateral extent of this domain is observed until the topography of the structure significantly diminishes, about 10 m outward to the top of the wall structure. The adjacent resistivity markedly differs towards higher resistivity (resistivity domain d), indicating a material change towards the moat and below 7–9 m depth. Therefore, the low resistivity domain is interpreted as an earthen structure on top of the original material. This structure with lateral change might represent a dam construction. Also, the shallow high resistivity of the brick structure was not found below elsewhere. Therefore, we agreed with the interpretation of the Fine Arts Department (2012) that the PWT earthwork was topped by the brick wall. In this case, we assume that the people of Nan built the earthwork and moat first. Then, they used the earthwork as a base of the wall and built the brick wall on the top. After that, they covered the bricks with clay soil to form the massive dam-like structure. Moreover, we hypothesized that the people in Nan have been intentionally covered the brick wall structure with earth due to the warfare reason. The brick wall alone can easily breach by cannon fire, which was introduced to warfare during this time. Covering by earth could potentially help to decrease the force of cannonballs since it must penetrate the earth layer first. Hence, our ERT data support the hypothesis of Lertrit (2000) that the people of Lanna lived in walled settlements, the earthwork reinforced the brick structure inside to make a stronger wall to prevent from enemies.

Ng et al. (2015) suggest the reason for building city walls during the Lanna period may also be related to flood mitigation since the ancient human settlements in northern Thailand had a linear pattern following the river. Therefore, such earthworks must be forceful enough to resist the high velocity of the water during overbank flow to halt persisting floods and protect the city area. A wall with a dam-like appearance can also be built for water management purposes. Due to the proximity of a Nan River meander at the PWT site, the wall may have served for the flood protection of the city. In accordance with the AD 1954 aerial photo, the end of the PWT wall site abutted the Nan River meander.

From the results derived here, we deduce two independent construction phases of Nan's ancient city walls. According to OSL dating, the MHW wall was constructed during the reign of King Ananta Woraritthi Det (AD 1855–1891; Fig. 8). Historical papers document that he requested permission from King Rama IV of Siam to relocate the city from Wiang Neau to its previous location of Wiang Tai in AD 1854 (Pharitdet 1918). In contrast, the PWT wall was apparently constructed around the period of the first lost war with Burma. Lanna has been slowly declining, especially after the death of King Tilokaraj in AD 1487 (Lertrit 2000; Nokngam 2018) and was finally lost to King Bayinnaung in AD 1558, when it became under Burmese control for 200 years (Ongsakul 2005). According to OSL dating, the bricks at the PWT site could probably fall into the reign of King Chao Phra Ya Phonthep Ruechai (AD 1527–1558), who was forced to abdicate after losing to Burma in AD 1558 (Pharidet 1918). Nan and the other cities in Lanna acted as the buffer state between Burma and Ayutthaya from 16th – nineteenth century AD (Lertrit 2000) and also attempted for liberation from Burma. The possibility of a coming war could be the reason to renovate the city wall to protect the city.

We deduce three potential reasons for the building of the Nan city wall in the nineteenth century. Defensive purposes should be considered as warfare in the region still used traditional elements such as war elephants until the nineteenth century (Bowie 2000; Charney 2018; Nossov 2012). Flood protection is a potential other reason. The wall confined the old town area which contained the several historical sites, temples, and the palace. The constructed wall covered this important landmark and would have helped to limit the effects of potential floods. However, cultural conservatism might also have played an important role. The ancient city Nan at the 5th location seems to have been constructed according to local cultural preferences, as according to Thongngern et al. (2007), King Ananta Woraritthi Det attempted to reconstruct the city according to the original structure of Wiang Tai (3rd location of Nan ancient city). The king still demanded to use the pattern of the city wall from Lanna period and constructed the moats along the wall to confine the limited area.

This study highlights the potential of combining geophysical surveys with luminescence dating to gain a deeper understanding of complex archaeological sites. In our case ERT provided crucial data, allowing us to analyse buried archaeological features and their properties across a large area. The ERT data facilitated informed decision-making. It helped us prior sample collection and identify specific features, such as an earthwork reinforced with brick and covered with clay, a feature observed in other Lanna cities and elsewhere in Asia (Stark 2006; Wood et al. 2015). OSL dating of bricks allowed to directly date the age of the wall

structures, unlike the other dating methods (e.g. radiocarbon), which often struggle with the lack suitable material and may yield unreliable ages (e.g. Srisunthon et al. 2022).

Conclusions

Ancient city wall constructions in SE Asia generally reflect several concepts related to cultural preference and environmental factors. Two sites in the city of Nan were studied in terms of both structure and brick chronology using ERT and OSL, respectively. The results of the ERT survey at the PWT site suggest that the lateral structure discovered could be related to dam construction. OSL dating results reveal two different phases of construction. The city wall at PWT was possibly built because of the war with Burma during sixteenth century AD. The MHW wall was constructed after the city relocated from Wiang Neau to Wiang Tai in the nineteenth century AD. The settlement morphology of the city wall surrounded by moats was implanted in mainland SE Asia until the nineteenth century AD. Our study also highlights the advantages of using ERT and OSL dating in tandem, providing a more comprehensive understanding of complex archaeological sites. We recommend this combined approach as a foundation for future archaeological work, enabling a better understanding and interpretation of the sites.

Supplementary Information The online version contains supplementary material available at <https://doi.org/10.1007/s12520-024-01984-9>.

Acknowledgements We would like to thank the Fine Arts Department of Thailand (Local Office No. 7) for providing data and permission for sampling. We thank Mr. Phonphayuha Chaiyarot, an archaeologist from the Fine Arts Department for the addition data about the site and the brick production. We would like to thank the Department of Geological Sciences at Chiang Mai University, Asst. Prof. Dr. Suwimon Udphuay, Mr. Adul Yawichai, Ms. Pattamas Nooliem and Mr. Panyawat Suriyapor for supplying the equipment for the geophysical investigation and surveying. We thank Mr. Pranot Rattana for help and support of logistical arrangements. We would like to thank the local people at the PWT and PPY site for supporting the sample collection. Furthermore, we thank Mr. Alex Fülling for guidance and assistance regarding sample preparation and Mr. William McCreary for reviewing an earlier version of the manuscript

Author contribution P. Srisunthon, D. Mueller and J. Wilk conducted fieldwork. P. Srisunthon, D. Mueller and F. Preusser conducted OSL dating. P. Srisunthon prepared the manuscript draft and figures 1–4 and 7–8. J. Wilk wrote the geophysical survey part and prepared figures 5–6. All authors contributed to the main text and reviewed the manuscript.

Funding Open Access funding enabled and organized by Projekt DEAL. This research is funded by the German Science Foundation through grant PR 957/5–1. J. Wilk received a grant by the German Science Foundation through grant WI 5667/1–3. P. Srisunthon received a grant by the German Academic Exchange Service, 57440921.

Data availability Data will be made available upon reasonable request.

Declarations

Competing interests The authors declare no competing interests.

Open Access This article is licensed under a Creative Commons Attribution 4.0 International License, which permits use, sharing, adaptation, distribution and reproduction in any medium or format, as long as you give appropriate credit to the original author(s) and the source, provide a link to the Creative Commons licence, and indicate if changes were made. The images or other third party material in this article are included in the article's Creative Commons licence, unless indicated otherwise in a credit line to the material. If material is not included in the article's Creative Commons licence and your intended use is not permitted by statutory regulation or exceeds the permitted use, you will need to obtain permission directly from the copyright holder. To view a copy of this licence, visit <http://creativecommons.org/licenses/by/4.0/>.

References

- Adams WH (2003) The Importance of Understanding Time Lag in the Acquisition, Curation, Use, and Disposal of Artifacts. *Hist Archaeol* 37:38–64
- Alves C, Sanjurjo-Sánchez J (2015) Conservation of stony materials in the built environment. *Environ Chem Lett* 13:413–430
- ASTER (2019) Global Digital Elevation Model v003 (NASA/METI/AIST/Japan SpaceSystems, and U.S./Japan ASTER Science Team). NASA EOSDIS Land Processes DAAC. <https://lpdaac.usgs.gov/products/astgtmv003/>. Accessed 15 Mar 2022
- Bailiff IK (2007) Methodological developments in the luminescence dating of brick from English late-medieval and post-medieval buildings. *Archaeometry* 49:827–851
- Blain S (2010) An application of luminescence dating to building archaeology: The study of ceramic building materials in early medieval churches in south-eastern England and north-western France. *Arqueología De La Arquitectura* 7:43–66
- Boomgaard P (2007) Southeast Asia: an environmental history. ABC-CLIO, California
- Bowie KA (2000) Ethnic Heterogeneity and Elephants in Nineteenth-Century Lanna. In: Turton A (ed) *Civility and Savagery: Social Identity in Tai States*, 1st edn. Curzon Press, Richmond, pp 330–348
- Boyd WE, McGrath RJ, Higham CF (1999) The geoarchaeology of Iron Age “moated” sites of the Upper Mae Nam Mun Valley, NE Thailand. I: Palaeodrainage, site–landscape relationships and the origins of the “moats.” *Geoarchaeology* 14:675–716
- Bray H, Bailey R, Stokes S (2002) Quantification of cross-irradiation and cross-illumination using a Risø TL/OSL DA-15 reader. *Radiat Meas* 35:275–280
- Charney M (2018) *Southeast Asian Warfare, 1300–1900*. Brill, Leiden
- Cheewinsiriwat P (2013) The use of GIS in exploring settlement patterns of the ethnic groups in Nan, Thailand. *Asian Ethnicity* 14:490–504
- Costas I, Reimann T, Tsukamoto S, Ludwig J, Lindhorst S, Frechen M, Hass HC, Betzler C (2012) Comparison of OSL ages from young dune sediments with a high-resolution independent age model. *Quat Geochronol* 10:16–23
- Degering D, Degering A (2019) ADELEv2017 Manual & Tutorial. https://adele.add-ideas.de/ADELEv2017_manual_v2.pdf. Accessed 1 Mar 2022
- Degering D, Degering A (2020) Change is the only constant-time-dependent dose rates in luminescence dating. *Quat Geochronol* 58:101074
- Duke B, Chang NJ, Moffat I, Morris W (2016) The invisible moats of the Mun River Valley, NE Thailand: the examination of water management devices at mounded sites through Ground Penetrating Radar (GPR). *J Indo-Pacific Archaeol* 40:1–11
- Fine Arts Department (2012) Report: The Excavation of Nan Ancient City Wall in Wat Phra Ya Wat Area (in Thai). Ploy Kan Pim, Chiang Mai
- Fine Arts Department (1993) Report: The Excavation and Renovation of Nan ancient city wall (in Thai). Fine Arts Department (Chiang Mai Office), Chiang Mai
- Galbraith RF, Roberts RG, Laslett GM, Yoshida H, Olley JM (1999) Optical dating of single and multiple grains of quartz from Jimmum rock shelter, northern Australia: Part I, experimental design and statistical models. *Archaeometry* 41:339–364
- Google Earth (2021) Imagery from 6th January 2021 (Maxar Technologies). <http://earth.google.com>. Accessed 15 Mar 2022
- Higham CFW (2011) The Iron Age of the Mun Valley, Thailand. *Antiqu J* 91:101–144
- Jacobs Z, Roberts R (2008) Advances in optically stimulated luminescence dating of individual grains of quartz from archaeological deposits. *Evol Anthropol* 16(6):210–223
- Janbuala S, Wasanapiarnpong T (2015) Effect of rice husk and rice husk ash on properties of lightweight clay bricks. *Key Eng Mater* 659:74–79
- Kreutzer S, Schmidt C, Fuchs MC, Dietze M, Fischer M, Fuchs M (2012) Introducing an R package for luminescence dating analysis. *Ancient TL* 30:1–8
- Laichen S (2003) Military technology transfers from Ming China and the emergence of Northern Mainland Southeast Asia (c. 1390–1527). *J Southeast Asian Stud* 34(3):495–517
- Lertlum S (2019) The Ancient Water Management Systems in Thailand. *Int J Geoinform* 15:37–48
- Lertrit S (2000) Cultural resource management and archaeology at Chiang Saen, Northern Thailand. *J Southeast Asian Stud* 31:137–161
- Liritzis I, Singhvi AK, Feathers JK, Wagner GA, Kadereit A, Zacharias N, Li S-H (2013) Luminescence dating in archaeology, anthropology, and geoarchaeology: an overview. Springer, Heidelberg
- McGrath R, Boyd WE (2001) The chronology of the Iron Age ‘moats’ of northeast Thailand. *Antiquity* 75:349–360
- Miksic JN, Goh GY (2017) *Ancient Southeast Asia*. Routledge, New York
- Moropoulou A, Zacharias N, Deleghou E, Apostolopoulou M, Palamara E, Kolaiti A (2018) OSL mortar dating to elucidate the construction history of the Tomb Chamber of the Holy Aedicule of the Holy Sepulchre in Jerusalem. *J Archaeol Sci Rep* 19:80–91
- Mudar K (1999) Mudar, K. M. (1999). How many Dvaravati kingdoms? Locational analysis of first millennium AD moated settlements in central Thailand. *J Anthropol Archaeol* 18:1–28
- Murphy SA (2013) Buddhism and its relationship to Dvaravati period settlement patterns and material culture in northeast Thailand and central Laos c. sixth–eleventh centuries AD: A historical ecology approach to the landscape of the Khorat Plateau. *Asian Perspectives*. 300–326
- Murray AS, Wintle AG (2000) Luminescence dating of quartz using an improved single-aliquot regenerative-dose protocol. *Radiat Meas* 32:57–73
- Negri S, Leucci G, Mazzone F (2008) High resolution 3D ERT to help GPR data interpretation for researching archaeological items in a geologically complex subsurface. *J Appl Geophys* 65:111–120
- Nelson MS, Rittenour TM (2015) Using grain-size characteristics to model soil water content: application to dose-rate calculation for luminescence dating. *Radiat Meas* 81:142–149

- Ng S, Wood SH, Ziegler AD (2015) Ancient floods, modern hazards: the Ping River, paleofloods and the 'lost city' of Wiang Kum Kam. *Nat Hazards* 75:2247–2263
- Nokngam A (2018) A relationship between Nan Sukhothai and Lanna in 14th - 17th century from archaeological evidence. Dissertation, Silpakorn University
- Nossov KS (2012) *War Elephants*. Osprey Publishing, Oxford
- Ongsakul S (1996) *Local Script of Nan: Phuen Muang Nan Chabab Wat Phra Koed* (in Thai). Amarin Printing and Publishing Public Company Limited, Bangkok
- Ongsakul S (2005) *History of Lanna* (Translated by Chitraporn Tanranakul). Silkworm Books, Chiang Mai
- O'Reilly DJ, Scott G (2015) Moated sites of the Iron Age in the Mun River Valley, Thailand: new discoveries using Google Earth. *Archaeol Res Asia* 3:9–18
- O'Reilly DJ (2008) Multivallate sites and socio-economic change: Thailand and Britain in their Iron Ages. *Antiquity* 82:377–389
- Osella A, Mdl V, Lascano E (2005) 3D electrical imaging of an archaeological site using electrical and electromagnetic methods. *Geophysics* 70:G101–G107
- Pailoplee S, Won-In K, Chaisuwana B, Charusiri P (2016) Thermoluminescence and optically stimulated luminescence dating of bricks from the Thung Tuk archaeological site, Southern Thailand. *Songklanakarinn J Sci Technol* 38:699–705
- Parry JT (1992) The investigative role of Landsat-TM in the examination of pre- and proto-historic water management sites in Northeast Thailand. *Geocarto Int* 7:5–24
- Pharitdet S (1918) *Historical Annals (Pongsawadan Muang Nan) Vol 10* by Phra Chao Suriyaphong Pharitdet (in Thai). Samosorn, Nan
- Phetsuriya N, Heath T (2021) Defining the Distinctiveness of Urban Heritage Identity: Chiang Mai Old City. *Thailand Social Sciences* 10:101
- Powell R, Hergt J, Woodhead J (2002) Improving isochron calculations with robust statistics and the bootstrap. *Chem Geol* 185:191–204
- Preusser F, Degering D, Fuchs M, Hilgers A, Kadereit A, Klasen N, Krbetschek M, Richter D, Spencer JQ (2008) Luminescence dating: basics, methods and applications. *E&G Quat Sci J* 57:95–149
- Rhodes E (2000) Observations of thermal transfer OSL signals in glacial quartz. *Radiat Meas* 32:595–602
- Schwarcz HP (1994) Current challenges to ESR dating. *Quatern Sci Rev* 13:601–605
- Scott G, O'Reilly D (2015) Rainfall and circular moated sites in north-east Thailand. *Antiquity* 89:1125–1138
- Smith ML (2003) Early walled cities of the Indian subcontinent as "small worlds." In: Smith ML (ed) *The social construction of ancient cities*, edn. Smithsonian Institution, Washington DC, pp 269–289
- Srinurak N, Mishima N (2017) Urban Axis and City shape evaluation through spatial configuration in 'Lan Na' Northern Thailand Historic city. *City, Territory Archit* 4:1–18
- Srisunthon P, Mueller D, Preusser F (2022) Decline of Lanna ceramic group production in northern Thailand (Ban Bo Suak site) confined by radiocarbon and luminescence dating. *Archaeol Anthropol Sci* 14:1–22
- Stark MT (2006) Early Mainland Southeast Asian Landscapes in the First Millennium A.D. *Annu Rev Anthropol* 35:407–432
- Stuart-Fox M (2021) *A short history of China and Southeast Asia: tribute, trade and influence*. Allen & Unwin, Crows Nest
- Supajanya T, Vallibhotama S (1972) The need for an inventory of ancient sites for anthropological research in northeastern Thailand. *Japan J Southeast Asian Stud* 10:284–297
- Sutas J, Mana A, Pitak L (2012) Effect of rice husk and rice husk ash to properties of bricks. *Procedia Eng* 32:1061–1067
- Thai Meteorological Department (2022) Rainfall accumulation of northern Thailand. http://climate.tmd.go.th/gge/Gra_AccumRain.pdf. Accessed 1 Dec 2023
- Thongngern S, Songmueang-kaen Y, Chaiwatanakul S (2007) *Nan City Wall* (in Thai). Department of Culture of Nan, Nan
- Vallibhotama S (1986) The ancient settlements of Sukhothai. a Conference on Thai Studies in Honor of William J. Gedney. 231–238
- Verdonck L, De Smedt P, Verhegge J (2019) Making sense of anomalies: Practices and challenges in the archaeological interpretation of geophysical data. In: Persico R, Piro S, Linford N (eds) *Innovation in Near-Surface Geophysics*, 1st edn. Elsevier, pp 151–194
- Welch DJ, McNeill JR (1988) Excavations at Ban Tamyae and Non Ban Kham, Phimai Region, Northeast Thailand. *Asian Perspect* 28:99–123
- White JC, Pigott VC (1996) From Community Craft to Regional. Craft specialization and social evolution: in memory of V. Gordon Childe 93:151
- Williams-Hunt PDR (1950) Irregular Earthworks in Eastern Siam: an air survey. *Antiquity* 24:30–36
- Wintle AG, Murray AS (2006) A review of quartz optically stimulated luminescence characteristics and their relevance in single-aliquot regeneration dating protocols. *Radiat Meas* 41:369–391
- Wood SH, Wood LR, Ziegler AD (2015) Natural degradation of earthworks, trenches, walls and moats, Northern Thailand. *J Field Archaeol* 40:675–694
- Wood R, Jacobs Z, Vannieuwenhuysse D, Balme J, O'Connor S, Whittau R (2016) Towards an accurate and precise chronology for the colonization of Australia: the example of Riwi, Kimberley. *Western Australia Plos One* 11:e0160123
- Wunderlich T, Wilken D, Erkul E, Rabbel W, Vött A, Fischer P, Hadler H, Heinzelmann M (2018) The river harbour of Ostia Antica-stratigraphy, extent and harbour infrastructure from combined geophysical measurements and drillings. *Quatern Int* 473:55–65
- Wyatt DK, Wichienkeo A (1995) *The Chiang Mai Chronicle*. Silkworm Books, Chiang Mai

Publisher's Note Springer Nature remains neutral with regard to jurisdictional claims in published maps and institutional affiliations.